Green Chemistry

Accepted Manuscript

ROYAL SOCIETY OF CHEMISTRY

www.rsc.org/greenchem

Green Chemistry

ARTICLE

Self-activation for activated carbon from biomass: Theory and parameters†

Received 00th January 20xx,
Accepted 00th January 20xx

DOI: 10.1039/x0xx00000x

www.rsc.org/greenchem

Changlei Xia and Sheldon Q. Shi*

Self-activation is a process that takes advantage of the gases emitted from the pyrolysis process of biomass to activate the converted carbon, which saves the cost of activating agents and decreases the environmental impact, as compared with conventional activation processes. An activation model was developed to describe the mechanism of the activation process, and it was examined by the self-activation experiments using kenaf core as a raw material. The relationships among the parameters, yields, specific surface areas, and specific pore volumes were quantified. The results showed that the ideal temperatures for the self-activation process of kenaf core were found between 970 – 1,090°C. The yield of 9.0% for the activated carbon from kenaf core provided a highest surface area per gram of biomass, while the yields of 5.5 – 13.8% could achieve 90% of the highest. The developed activation model can be used to explain the relationship between the yields, specific surface areas, and specific pore volumes, effectively.

Introduction

Activated carbon is a crude form of graphite with a random or amorphous structure, which is highly porous with a large internal surface area (*SA*).[1] Various uses of activated carbon include purification,[2] porous-supported catalysts,[3-6] hydrogen storage capacity,[7,8] and battery.[9,10] The American Water Works Association (AWWA) B600 standard requires that the activated carbon has a specific surface area (*SSA*) in excess of 500 m^2 g^{-1} determined by N_2 adsorption at 77 K.

The process for activated carbon includes two steps, carbonization for the conversion of carbonaceous substances into carbon, and activation for the *SSA* and specific pore volume (*SPV*) increase of the converted carbon. The carbonaceous materials are usually pyrolyzed at temperatures between 600 – 900°C in an inert atmosphere for the carbonization, followed by the activation process.[1] Activation methods can be divided into two categories: (1) physical/thermal activation, and (2) chemical activation.[1] Physical/thermal activation uses a mild oxidizing gas, such as CO_2 or water steam,[1] to eliminate the bulk of the volatile matters, followed by partial gasification. The chemical activation method employs chemicals (such as acid, strong base, or salt) to increase the SSA, e.g. zinc chloride ($ZnCl_2$),[11] potassium hydroxide (KOH),[12] sodium hydroxide (NaOH),[13] nitric acid (HNO_3),[14] sulfuric acid (H_2SO_4),[15] hydrochloric acid (HCl),[16] hydrogen peroxide (H_2O_2),[17] phosphoric acid (H_3PO_4),[18] potassium carbonate (K_2CO_3),[19] potassium phosphate dibasic (K_2HPO_4),[20] and cobalt acetate ($Co(OAc)_2$).[21] In the traditional activation process, physical activation using CO_2 and chemical activation using $ZnCl_2$ are two common methods. Both methods introduce additional gas (CO_2) or a chemical ($ZnCl_2$), from which both the CO_2 emission from the activation process and the zinc compound removal by acid from the follow-up process will cause environmental concerns.

Self-activation process of biomass was first disclosed in our patent,[22] which takes advantage of the gases emitted from the biomass during the carbonization process to serve as the activating agent, so that the carbonization and activation are combined into one step. A recent publication bearing the name "self-activation",[23] presented a one-step pyrolysis of cellulose for activated carbon. A flowing argon was employed during the process. In the technology described in this paper, no gas was introduced during the self-activation process. The activated carbon fabricated through self-activation process presented high specific surface area (up to 2432 m^2 g^{-1}), which is comparable with that manufactured by the conventional activation processes (up to 1926 m^2 g^{-1} for the physical activation, and 1642 m^2 g^{-1} for the chemical activation).[24] Compared to the conventional activated carbon manufacturing, the cost of activating agents is saved using the self-activation technology, since no activating gas or chemical is used. In addition, the self-activation process is more environmentally friendly. The exhaust gases (CO and H_2) can be used as fuel or as feedstock for methanol production with further synthesis. To understand the mechanism of the self-activation process, a novel model is developed. The parameters (i.e. temperature, dwelling time, air, and moisture) affecting the self-activation are evaluated, and the changes of *SSA* and (*SPA*) on the yield of the self-activation are elucidated.

Department of Mechanical and Energy Engineering, University of North Texas, Denton, TX 76203, USA. E-mail: Sheldon.Shi@unt.edu
† Electronic Supplementary Information (ESI) available. See DOI: 10.1039/x0xx00000x

Results and discussion

Theory of self-activation

It was reported that the pyrolysis gases from biomass mainly contained H_2, CO_2, CO, CH_4, H_2O, etc.[23,25] in which CO_2 and H_2O have been widely used to serve as activating agents in the activated carbon production.[1,26] Therefore, the CO_2 and H_2O in the pyrolysis gases may activate the carbon, so that no additional gas needs to be introduced.

To demonstrate the self-activation process, one type of biomass, kenaf core (Biotech Mills Inc., USA, 3 – 30 meshes, 11.7% moisture content based on the ASTM D4442 standard), was used in a designed experiment. The dried kenaf core contains 49.0% cellulose, 29.7% hemicellulose, and 19.2% lignin,[27] from which has 82.85% volatile matter (ASTM E872 standard), 15.41% fixed carbon, and 1.74% ash (ASTM E1755 standard). Carbon, hydrogen, oxygen, nitrogen, and sulfur contents of kenaf core were found to be 48.00%, 6.37%, 42.10%, 0.35%, and 0.07%, respectively (see Table S1 in the ESI†).[28] After self-activation at 1,000°C for 10 h, the resulted activated carbon contains 0.68% volatile matter (ASTM D5832 standard), 80.47% fixed carbon, and 18.85% ash (ASTM D2866 standard). The contents of carbon, hydrogen, oxygen, nitrogen, and sulfur of the resulted activated carbon were measured as 92.14%, 0.54%, 0.12%, 0.16%, and 0.02%, respectively (see Table S1 in the ESI†).

From the ultimate analysis of the kenaf core, the chemical formula was found as $(C_{4.00}H_{6.32}O_{2.63})_n$. An equilibrium reaction of the pyrolysis of 179 g (equal to 1.86 mol of $C_{4.00}H_{6.32}O_{2.63}$) dried kenaf core was calculated from the FactSage software and databases and shown in reaction (1).[29]

$$1.86C_{4.00}H_{6.32}O_{2.63}(s) \xrightarrow{1{,}000^{\circ}C,\ 1atm} \begin{matrix} 2.57C(s) + 5.77H_2(g) + \\ 4.82CO(g) + 0.03H_2O(g) + \\ 0.03CH_4(g) + 0.02CO_2(g) + \cdots \end{matrix} \quad (1)$$

The pyrolysis condition was set as 1,000°C in temperature and 1 atm in pressure. From reaction (1), the yield of carbon at the equilibrium was obtained as 17.18% (2.57 mol), and the gas products resulting from the pyrolysis process were mainly H_2 (5.77 mol) and CO (4.82 mol). Mass spectrometry (MS) and Fourier transform infrared spectroscopy (FT-IR) were performed on the gases emitted from the self-activation process (see Figs. S1 and S2, and Table S2 in the ESI†) to conform the reaction (1). The MS results showed that the gas components include CO, CO_2, H_2, H_2O, CH_4, and etc. The FT-IR results showed that the FT-IR absorbance of CO/CO_2 was increased by 128.8% when the dwelling time (pyrolysis temperature: 1,000°C) increased from 2 h to 30 h, indicating that CO_2 was reacted with C as an activating agent to generate CO. Based on the activation theory, experiments were carried out using the self-activation process (details in Experimental).

Effectiveness of self-activation

The self-activation process was conducted on different biomass types, including kenaf fibre, kenaf core, sugarcane, sugarcane bagasse, sugarcane leaf, coconut fibre, peanut shell, and sawdust. A comparative experiment was conducted between the self-activation and non-activation (details in Methods summary). Self-activation and non-activation were carried out in the same conditions except that for the self-activation, the material was activated by the emitted gases. The Brunauer–Emmett–Teller (BET) specific surface area (SSA_{BET}) results for different biomass types pyrolyzed at 1,100°C for 2 hours with self-activation or non-activation were:

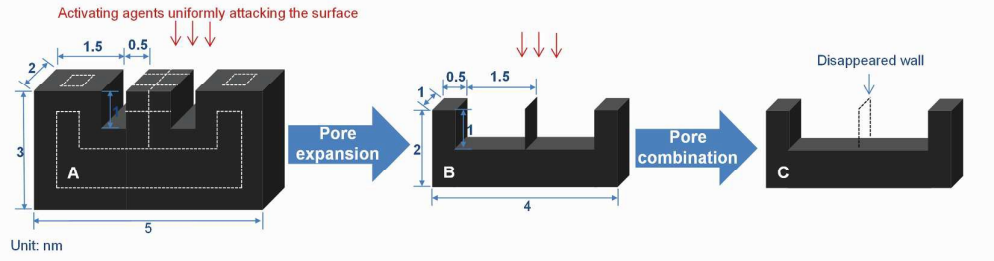

Status	A	Pore expansion	B	Pore combination	C
SA (nm²)	68	↓58.8%	26	↓7.7%	24
PV (nm³)	2	↑50.0%	3	~0%	3
V (nm³)	28	↓82.1%	5	~0%	5
SSA (nm² g⁻¹)	2.4/*D*	↑114.1%	5.2/*D*	↓7.7%	4.8/*D*
SPV (nm³ g⁻¹)	0.071/*D*	↑8400%	0.6/*D*	~0%	0.6/*D*

Notes: *SA* = surface area; *PV* = pore volume; *V* = volume; *SSA* = specific surface area, equal to *SA*/(*VD*); *SPV* = specific pore volume, equal to *PV*/(*VD*); *D* = Density of carbon, assuming to be constant.

Fig. 1 Illustration of the activation model. A carbon particle (A) (overall dimensions: 2 × 3 × 5 nm) with two pores (dimensions: 0.5 × 1 × 2 nm) was employed for the demonstration. After the pore expansion process (A to B), the SSA and SPV are increased by 114.1% and 8400%, respectively. After the pore combination process (B to C), the SSA is reduced by 7.7% and the SPV remains constant.

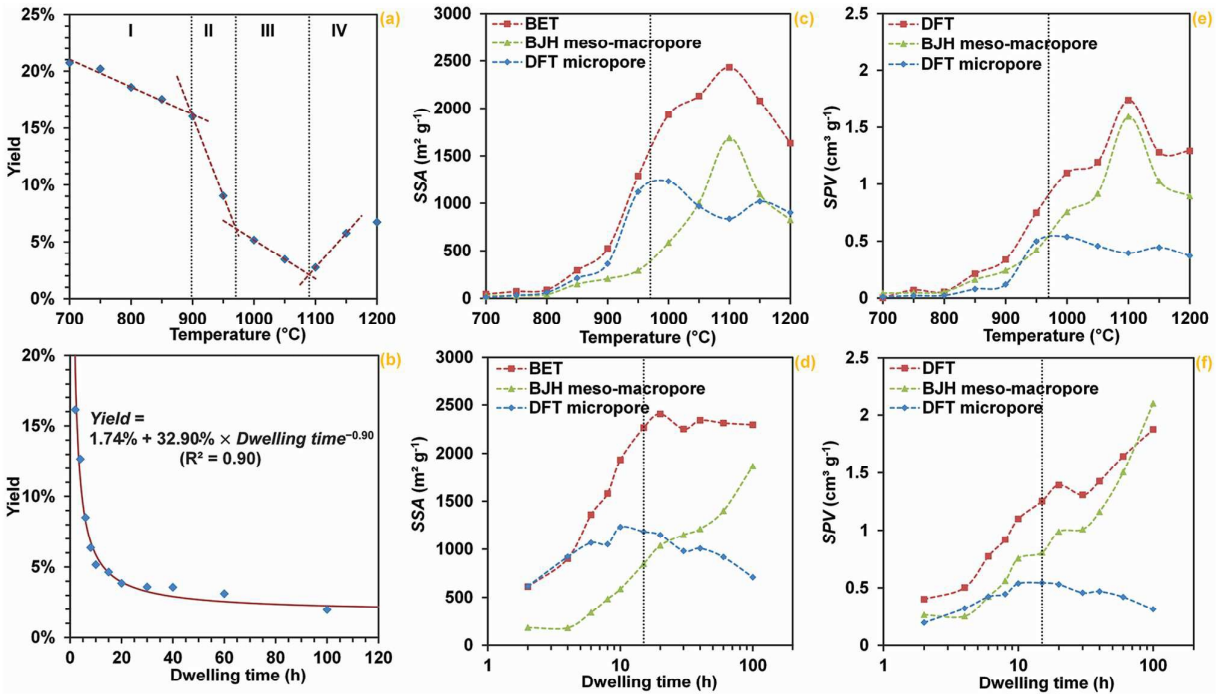

Fig. 2 Temperature-dependent changes (pyrolysis time: 10 hours) of a) yield, c) *SSA* and e) *SPV*, and dwelling time-dependent changes (pyrolysis temperature: 1,000°C) of b) yield, d) *SSA* and f) *SPV*.

kenaf bast fibre ($SSA_{BET/Self\text{-}activation}$: 1,280 m^2 g^{-1}; $SSA_{BET/Non\text{-}activation}$: 252 m^2 g^{-1}; Increment: 408%), kenaf core (1,148 m^2 g^{-1}; 168 m^2 g^{-1}; 583%), sugarcane bagasse (910 m^2 g^{-1}; 349 m^2 g^{-1}; 161%), sugarcane leaf (591 m^2 g^{-1}; 155 m^2 g^{-1}; 281%), coconut fibre (1,413 m^2 g^{-1}; 264 m^2 g^{-1}; 435%), peanut shell (722 m^2 g^{-1}; 84 m^2 g^{-1}; 760%), and sawdust (1,199 m^2 g^{-1}; 354 m^2 g^{-1}; 239%). The activated carbon fabricated from the self-activation process presents a *SSA* greater than the minimum requirement (500 m^2 g^{-1}) in accordance with the AWWA B600 standard. The results showed that the emitted gases had served as activating agents for the converted carbon from the biomass.

An activation model

A number of models were developed to describe the activation process, such as kinetic models,[30-33] gradual activation model,[34] and random pore model (RPM).[35] However, these models have the limitations in explaining the changes of *SSA* and *SPV*. We developed a simplified model to describe the activation process as shown in Fig. 1. Gas activation is an oxidation process on the carbon surface to increase the *SSA*. We assume that the oxidations happen uniformly on the entire surface of the carbon. Two scenarios may happen during the activation process: 1) pore expansion (A to B in Fig. 1); and 2) pore combination (B to C in Fig. 1). The pores are combined through the removal of the thin borders between the pores. During the pore expansion process, the *SA* and pore volume (*PV*) of the carbon particle are reduced by 58.8% and increased by 25%, respectively. In the meantime, the *SSA* and *SPV* are increased by 114.1% and 8,400%, respectively, with a corresponding 82.1% volume reduction. During the pore combination (B to C), both the surface area and the *SSA* are reduced by 7.7%, while the *SPV* is approximately constant. It indicates that the pore combination has negatively effect on the *SSA,* but little effect on the *SPV*. In the activation process, the *SSA* is increased by pore expansion, but is decreased by pore combination, from which the total *SSA* maybe unchanged during the process. In general, for the change of *SSA*, pore expansion dominates during the early stage of the pyrolysis process. As the pyrolysis process continues, pore expansion and pore combination will be balanced until the pore combination is gradually dominating. Eventually, the material will be turned into ash. As the pore volume may not be affected by the pore combination, the *SPV* will keep increasing. Experiments were conducted to validate the developed activation model and are presented in a later section of the paper.

Pyrolysis parameters for self-activation

The effect of different pyrolysis parameters on the efficiency of the self-activation process was studied. Kenaf core was selected for the investigation of the self-activation process. The following pyrolysis parameters were investigated: pyrolysis temperature, dwelling time, air in the furnace, and moisture of the kenaf core.

Pyrolysis experiments were conducted on the kenaf core at different temperatures between 700 – 1,200°C with an interval

Table 1 The effects of the moisture of biomass and the air-free condition of the furnace on the yield and specific surface area of the self-activated carbon.

Dwelling time (h)		2			10			Equilibrium [a]		
Conditions	Moisture [c]	Yes	No	No	Yes	No	No	Yes	No	No
	Air [d]	Yes	Yes	No	Yes	Yes	No	Yes	Yes	No
Yield (%)		16.13	16.54	17.04	5.16	6.21	7.05	7.93	15.71	17.18
SSA_{BET} [b] ($m^2\ g^{-1}$)		611	558	507	1932	1825	1689	-	-	-

[a] Theory data, calculated by FactSage software. [b] SSA_{BET} = BET specific surface area. [c] 21 g moisture in 200 g kenaf core. [d] 11.8 L of air in the furnace (96.6% vacuum).

of 50°C, dwelling for 10 hours. The relationship between yield and pyrolysis temperature is shown in Fig. 2a. Four phases can be identified in Fig. 2a: I) 700 – 898°C, II) 898 – 970°C, III) 970 – 1,090°C, and IV) 1,090 – 1,200°C. High yields (20.73 – 16.24%) were obtained in Phase I. As the pyrolysis temperature increased, the yield decreased, and a slow self-activation was presented in Phase I. In Phase II, as the temperature increased from 898°C to 970°C, the yield continued to decrease, and the yield reduction became much more rapid (0.14 % $°C^{-1}$) compared to that in Phase I (0.023% $°C^{-1}$). In Phase III, the yield reduction rate decreased to 0.034% $°C^{-1}$, indicating that the temperature had less effect on the yield reduction. In Phase IV, the yield increased as the pyrolysis temperature increased. This could be explained that during Phase IV, the decomposition rate of gases into carbon exceeded the gasification rate of the carbon by the activating gases.

Fig. 2b indicates a relationship between the yield and the dwelling time at a pyrolysis temperature of 1,000°C. Fig. 2b shows that, as the dwelling time increased, the yield decreased rapidly at the initial stage and then slowed down until it levelled off. The process followed the exponential function:

$$Yield = 1.74\% + 32.90\% \times Dwelling\ time^{-0.90} \quad (2)$$

where 1.74% is the ash content determined based on the procedure described in ASTM E1755 standard. The coefficient of determination (R^2) for the equation (2) was 0.90.

The effects of pyrolysis temperature and dwelling time on the SSA_{BET}, *SSA* of Barrett–Joyner–Halenda (BJH) meso-macropore ($SSA_{BJH\ meso\text{-}macropore}$), *SSA* of Density Functional Theory (DFT) micropore ($SSA_{DFT\ micropore}$), *SPV* of DFT overall pores (SPV_{DFT}), *SPV* of BJH meso-macropore ($SPV_{BJH\ meso\text{-}macropore}$), and *SPV* of DFT micropore ($SPV_{DFT\ micropore}$) were investigated, and the results are shown in Fig. 2c-f. The changes of *SSA* and *SPV* as a function of pyrolysis temperature are shown in Fig. 2c and Fig. 2e, respectively. The SSA_{BET} of the activated carbon was lower than 500 $m^2\ g^{-1}$, when the kenaf core was pyrolyzed only in the stage of Phase I (Fig. 2a), i.e. 700, 750, 800, and 850°C. During the stage Phase II (898 – 970°C), the SSA_{BET} and $SSA_{DFT\ micropore}$ increased quickly. The quickest increase for $SSA_{BJH\ meso\text{-}macropore}$ happened in Phase III (970 – 1090°C). The $SSA_{DFT\ micropore}$ reached the maximum at around 970°C, indicating that the micropore started to be translated into mesopore by the pore expansion process. In Phase III (970 – 1090°C), SSA_{BET} increased slightly slower than that of the $SSA_{BJH\ meso\text{-}macropore}$, because the pores were changed from micropore to mesopore during the pore expansion process. In Phase IV (1090 – 1200°C), the $SSA_{DFT\ micropore}$ remained the same, while the SSA_{BET} and $SSA_{BJH\ meso\text{-}macropore}$ decreased. Similar trends were found for the SPV_{DFT}, $SPV_{BJH\ meso\text{-}macropore}$ and $SPV_{DFT\ micropore}$ (Fig. 2e).

The specific surface area (SSA_{BET}, $SSA_{BJH\ meso\text{-}macropore}$, and $SSA_{DFT\ micropore}$) changes as a function of dwelling time (at 1,000°C pyrolysis temperature) as shown in Fig. 2d. In general, SSA_{BET} increased during the first 15 h and then stabilized. The $SSA_{BJH\ meso\text{-}macropore}$ increased throughout the whole pyrolysis period. The $SSA_{DFT\ micropore}$ reached the maximum at around 10 hours and then decreased. The *SPV* changes ($SPV_{BJH\ meso\text{-}macropore}$, $SPV_{DFT\ micropore}$, and SPV_{DFT}) as a function of dwelling time are shown in Fig. 2f. As it is seen in Fig. 2f, the $SPV_{BJH\ meso\text{-}macropore}$ shows a similar trend to that of the $SSA_{BJH\ meso\text{-}macropore}$ (Fig. 2d). The $SPV_{DFT\ micropore}$ also shows a similar trend to that of the $SSA_{DFT\ micropore}$ (Fig. 2d). However, while the total surface area (SSA_{BET}) levels off at a certain dwelling time (about 15 hours), the total pore volume (SPV_{DFT}) continues to increase beyond the 15-hour dwelling time. This finding indicated that the pore expansion and pore combination was balanced at the dwelling time of about 15 hours. During the activation process, the micropore was expanded into the mesopore by the pore expansion. For the internal pores in the activated carbon, when the walls between the adjacent pores disappear because of the pore expansion, the *PV* will continue to increase, while the *SA* may be decreased. Therefore, the pore combination will have a significant effect to the *SPV* of micropore and the total *SSA*, but litter effect to the meso-macropore and total *SPV*. The results indicated that the pore combination would be minor when the meso-macropore were important for the activated carbon.

In order to investigate the effect of moisture in the biomass on the self-activation process, kenaf core with a moisture content of 9.1% was used for the pyrolysis experiments at an initial pressure of -97,906 ± 34 Pa (96.6% vacuum). From the ideal gas equation, around 11.8 L of air was estimated to remain in the furnace. The pyrolysis treatment were carried out at 1,000°C for 2 or 10 h on the kenaf core samples at three conditions: (1) 200 g (21 g moisture) in 11.8 L air condition, (2) 179 g (dried) in 11.8 L air condition, and (3) 179 g (dried) in air-free condition. The air-free condition was achieved by applying

vacuum and introducing argon into the furnace for three times. Before the pyrolysis experiments, the pressure in the furnace was kept at 96.6% vacuum with argon introduced. Table 1 shows the yield and SSA_{BET} of activated carbon processed at different conditions. When the other conditions remain the same, air and moisture in the furnace will accelerate the activation process of the materials (showing reduced yields and increased SSA_{BET}). The moisture and carbon dioxide in the air may serve as activating agents directly to activate the converted carbon, while the oxygen may react with biomass/converted carbon to form CO_2 as an activation agent, so that a self-activation process can be implemented. The more the activating agent generated in the furnace, the faster the self-activation process would be.

The estimated yields for the self-activation at equilibrium was calculated using the FactSage software. The results, as seen in Table 1, show that the estimated yields agree with the measured yield results from the experiments. There are about 21% O_2 in the atmospheric environment, which are about 0.11 mol O_2 in the 11.8 L air (estimated from 350 L of furnace in 96.6% of vacuum). During the self-activation processes, the reaction of kenaf core with moisture and 11.8 L air in the furnace was estimated by the FactSage software and shown in reaction (3):

$$1.86C_{4.00}H_{6.32}O_{2.63}(s) + 1.17H_2O(l) + 0.11O_2(g) \xrightarrow{1{,}000^{\circ}C,\ 1atm} 1.18C(s) + 6.92H_2(g) + 6.18CO(g) + 0.04H_2O(g) + 0.03CH_4(g) + 0.02CO_2(g) + \cdots \quad (3)$$

The reaction of dried kenaf core and 11.8 L air in the furnace is shown in reaction (4):

$$1.86C_{4.00}H_{6.32}O_{2.63}(s) + 0.11O_2(g) \xrightarrow{1{,}000^{\circ}C,\ 1atm} 2.34C(s) + 5.77H_2(g) + 5.03CO(g) + 0.03H_2O(g) + 0.03CH_4(g) + 0.02CO_2(g) + \cdots \quad (4)$$

As shown in Table 1, the yields of the activated carbon pyrolyzed for 10 hours were much less than the yields that were pyrolyzed for 2 hours. The longer the pyrolysis, the less the yield. However, Table 1 also indicates that the yields at equilibrium estimated from the FactSage software were greater than the measured yields pyrolyzed for 10 hours. The reasons for these results can be twofold: 1) during the pyrolysis process, the biomass materials are decomposed into small molecules, some of which are vaporized, which causes some carbon losses; and 2) since the activity of carbon (α) at the location of the sample is higher than that at other locations in the furnace, the reaction (5) goes reversely at the sample location, but not at the other locations. It was observed from the experiments that the inner surface of the furnace chamber was coated by a layer of carbon after the pyrolysis experiments.

$$2CO(g) \rightleftharpoons C(s) + O_2(g) \quad (5)$$

Yield-dependent surface areas and pore volumes

According to the SSA_{BET} data in Table 2, a relationship between $\ln(SSA_{BET})$ and the yield for the powdered activated carbon (PAC) was plotted and presented in Fig. 3a. A linear relationship was established as shown below with a R^2 of 0.98.

$$\ln(SSA_{BET}) = -11.14 \times Yield + 8.16 \quad (6)$$

Please be noticed that a few data points were excluded in the analysis. These data points were presented in high yield end (PACs (700-850°C, 10 h)), which did not agree with most of the main trends. Some volatile matters might still be in the carbon, as the total residue from the volatile test was 17.15% (including 15.41% fixed carbon and 1.74% ash), which was lower than the measured yield of PACs (700-850°C, 10 h), i.e. 17.54 – 20.73%. These volatile matters would occupy the pores of the carbon, resulting in a lower SSA_{BET} than that in the trend line (Fig. 3a). The abnormal data points at the low yield end (PAC (1,000°C, 100 h) and ash) were also excluded. The ash is an extreme case for the pyrolysis process with a minimum SSA_{BET}. For the PAC processed at 1,000°C, at 100 hours, the pore combination dominated the process (Fig. 1), resulting in the SA_{BET} reduction.

The efficiency of total surface area generation from kenaf core was analysed and presented in Fig. 3b. The surface area per gram kenaf core can be calculated by:

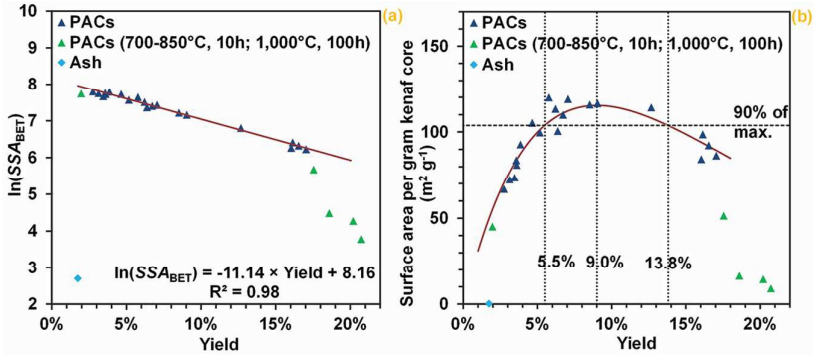

Fig. 3 The relationships between the yield and a) nature log of the SSA_{BET} and b) the surface area per gram of the kenaf core.

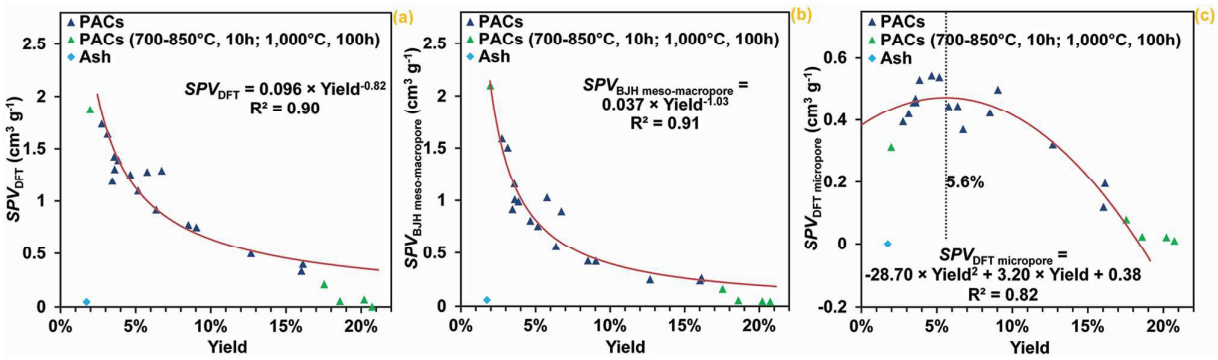

Fig. 4 The relationships between yield and *SPV* from the models of a) DFT; b) BJH meso-macropore; and c) DFT micropore.

$$Surface\ area\ per\ gram\ kenaf\ core = SSA_{BET} \times Yield \quad (7)$$

Combining equations (6) and (7), the relationship between surface area per gram kenaf core and yield can be obtained as:

$$Surface\ area\ per\ gram\ kenaf\ core = e^{-11.14 \times Yield + 8.16} \times Yield \quad (8)$$

Fig. 3b shows a comparison of the model estimates (equation (8)) and the measured data for the relationship between the surface area per gram of kenaf core and the yield. It can be concluded from Fig. 3b that the established model (equation (8)) is a good predictor for the unit surface area. Fig. 3b shows that the activated carbon from kenaf core with the yields between 5.5 – 13.8% are the most efficient in activated carbon production, from which the highest unit surface area (115 m^2 g^{-1}) of the PAC was obtained at the yield of 9.0%.

Usually, the larger the pore volume, the higher the capability of the activated carbon can be obtained to absorb the impurities. Absorptions for different sizes of the impurities require different pore volumes for the activated carbon. Micropores in the activated carbon tend to absorb small molecules (e.g. iodine), while meso-macropores absorb large molecules (e.g. tannic acid). Fig. 4 shows the relationships between the yields and the pore volumes for the three different pore volumes, including total pore volume (SPV_{DFT}), mesa-macropore volume ($SPV_{BJH\ meso\text{-}macropore}$), and micropore volume ($SPV_{DFT\ micropore}$). Again, the points of PACs (700-850°C, 10 h; 1,000°C, 100 h) and ash were not included in the analysis.

For the relationship between SPV_{DFT} and yield as shown in Fig. 4a, a power fitting equation was established as shown in equation (9).

$$SPV_{DFT} = 0.096 \times Yield^{-0.82} \quad (9)$$

SPV_{DFT} represents the total pore volume of micro-macropores.

The BJH model is applied to the analysis of meso-macropore volume. The calculation range of BJH was set to be 2 – 300 nm. As shown in Fig. 4b, a power fitting can also be applied to describe the data with an established equation shown in equation (10).

$$SPV_{BJH\ meso\text{-}macropore} = 0.037 \times Yield^{-1.03} \quad (10)$$

The micropore volume was analysed using the DFT model (Fig. 4c). It was noticed from Fig. 4c that some $SPV_{DFT\ micropore}$ data showed negative values, which were not realistic. A relationship between the micropore volume and the yield was established following the second order fitting as shown in equation (11).

$$SPV_{DFT\ micropore} = -28.70 \times Yield^2 + 3.20 \times Yield + 0.38 \quad (11)$$

The $SPV_{DFT\ micropore}$ reached a maximum when the yield was around 5.6%. Based on the proposed activation theory discussed in Fig. 1, the size of the pore increases during the activation process. When the pore size exceeds 2 nm, the pore is no longer considered a micropore. Therefore, at a certain point of activation, the micropore volume starts to decrease.

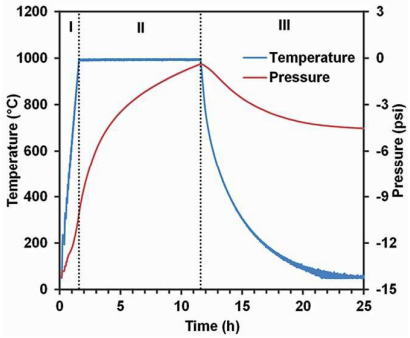

Fig. 5 The internal pressure and temperature as a function of time in three pyrolysis periods: I) ramping (10°C min-1); II) dwelling (for 10h); and III) controlled cooling (10°C min-1 and then self-cooling) to room temperature.

Experimental

Self-activation process

A high-temperature versatile box furnace (STY-1600C, Sentro Tech Corp., USA) was used to process the PAC. The furnace is equipped with a vacuum system and gas flow with a maximum temperature of 1,600°C. A type-k thermocouple with a data logger (TC101A, MadgeTech, Inc., USA) was used in the furnace to detect the internal temperature. A digital pressure gauge (ADT680W-25-CP15-PSI-N, Additel Corp., USA) was used to measure the pressure of the furnace chamber. The heat chamber of the furnace is made with alumina ceramic with dimensions of 254 × 254 × 305 mm^3. The total volume of furnace was estimated as 350 litres measured using argon at low pressure based on the ideal gas equation ($PV = nRT$).

The following procedure was used for the self-activation pyrolysis process: 1) Placed the biomass into the box furnace chamber; 2) Set the vacuum to a pressure of -97,906 ± 34 Pa (96.6% vacuum). The valves of the furnace were then turned off to create a closed system so that no mass exchanging occurred during the pyrolysis process; and 3) Conducted pyrolysis process following the three steps: a) ramping with a temperature-increasing rate of 10°C min^{-1}; b) dwelling, and c) cooling with a temperature-decreasing rate of no more than 10°C min^{-1} to room temperature (Fig. 5). The activated carbon products were then taken out from the furnace, and pulverized by an ultra-fine pulverizing machine (RT-UF26, Rong Tsong Precision Technology Co., Taiwan) to match the size requirement of PAC according with the AWWA B600 standard. The kenaf core based activated carbon sample was labelled as PAC (pyrolysis temperature, dwelling time), e.g. PAC (1,000°C, 10 h).

Non-activation process

For the specimens with self-activation, the biomass materials were placed inside the furnace with no cover which allowed the gases generated from the biomass to flow through the converted carbon material. For the specimens with non-activation, the biomass was put in a crucible, and a cap was used to cover the container so that limited gases would access the biomass materials. The biomass in the crucible (volume about 0.5 L) was pyrolyzed to generate gases, which flow out of the crucible to the furnace. When the pressure reached a balance inside and outside of the crucible, the gas exchange would stop. Thus, only a small amount of gases, 1.4% (0.5 L/350 L, crucible volume/furnace volume) remained in the crucible, which provided limited gas activation opportunity for the produced carbon, and was classified as non-activation.

Characterization

The adsorption capabilities of the PACs were determined by

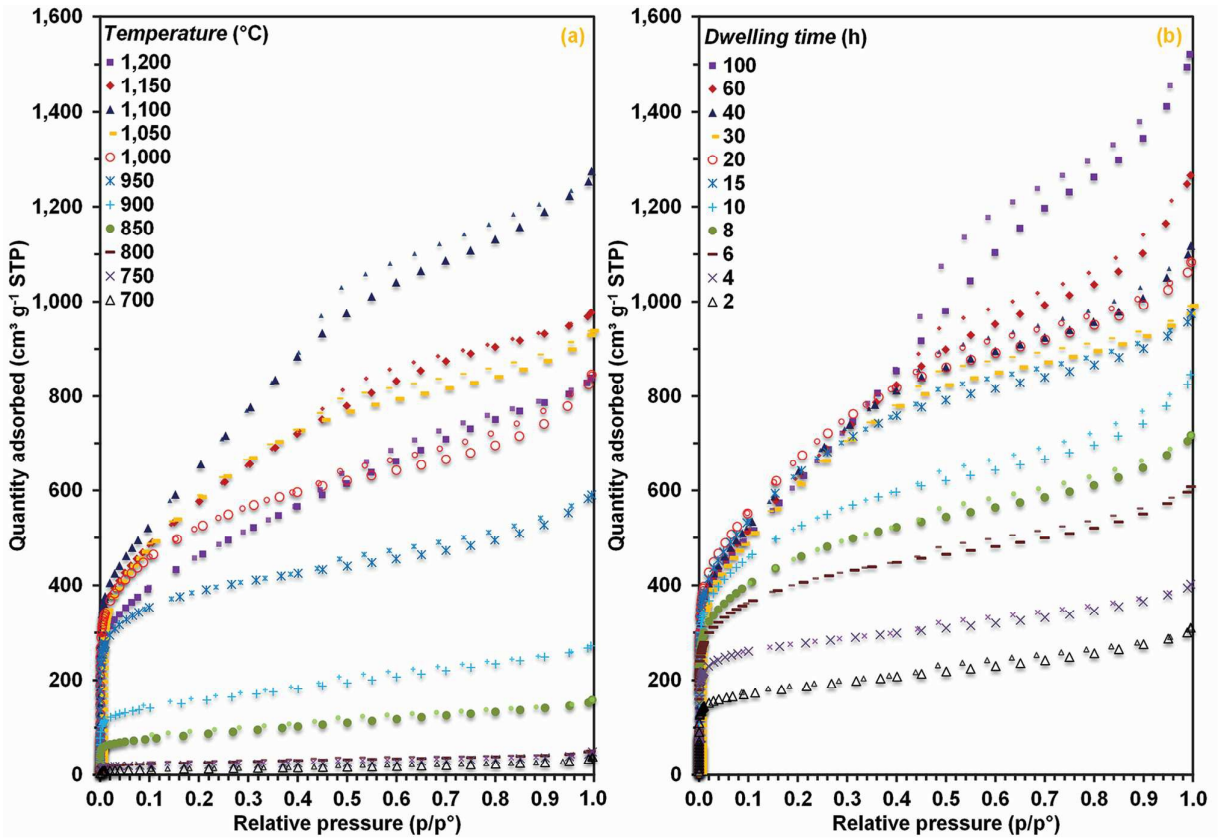

Fig. 6 Isothermal plots of PACs at a) pyrolysis temperatures from 700°C to 1,200°C (dwelling time: 10 h) and b) dwelling times from 2 h to 100 h (pyrolysis temperature: 1,000°C).

Table 2 *SSA* and *SPV* of PAC samples processed at different temperatures and dwelling times.

Sample	*Yield* (%)	SSA_{BET} [b] ($m^2\ g^{-1}$)	$SSA_{BJH\ meso\text{-}macropore}$ [c] ($m^2\ g^{-1}$)	$SSA_{DFT\ micropore}$ ($m^2\ g^{-1}$)	SPV_{DFT} [d] ($cm^3\ g^{-1}$)	$SPV_{BJH\ meso\text{-}macropore}$ ($cm^3\ g^{-1}$)	$SPV_{DFT\ micropore}$ ($cm^3\ g^{-1}$)
PAC (700°C, 10 h) [a]	20.73	44	27	12	0.003	0.044	0.010
PAC (750°C, 10 h)	20.20	72	29	31	0.070	0.047	0.022
PAC (800°C, 10 h)	18.59	89	40	62	0.055	0.055	0.024
PAC (850°C, 10 h)	17.54	293	149	212	0.212	0.161	0.079
PAC (900°C, 10 h)	16.03	526	206	363	0.337	0.241	0.119
PAC (950°C, 10 h)	9.04	1,289	291	1121	0.749	0.423	0.498
PAC (1,000°C, 10 h)	5.16	1,932	587	1232	1.099	0.755	0.538
PAC (1,050°C, 10 h)	3.45	2,132	1,003	970	1.194	0.916	0.457
PAC (1,100°C, 10 h)	2.75	2,432	1,688	837	1.740	1.593	0.395
PAC (1,150°C, 10 h)	5.77	2,080	1,095	1019	1.281	1.028	0.445
PAC (1,200°C, 10 h)	6.73	1,634	824	903	1.292	0.894	0.370
PAC (1,000°C, 2 h)	16.13	611	183	615	0.401	0.263	0.195
PAC (1,000°C, 4 h)	12.67	901	180	921	0.502	0.251	0.321
PAC (1,000°C, 6 h)	8.51	1,360	339	1066	0.773	0.424	0.424
PAC (1,000°C, 8 h)	6.37	1,580	483	1052	0.918	0.561	0.445
PAC (1,000°C, 15 h)	4.65	2,266	848	1185	1.253	0.805	0.543
PAC (1,000°C, 20 h)	3.85	2,408	1,038	1149	1.393	0.989	0.530
PAC (1,000°C, 30 h)	3.60	2,252	1,150	980	1.307	1.010	0.458
PAC (1,000°C, 40 h)	3.58	2,342	1,213	1008	1.425	1.161	0.469
PAC (1,000°C, 60 h)	3.13	2,314	1,400	918	1.644	1.505	0.421
PAC (1,000°C, 100 h)	1.97	2,296	1,866	709	1.876	2.100	0.313
Ash	1.74	15	16	0	0.047	0.059	0.000

[a] Powdered activated carbon (pyrolysis temperature, dwelling time). [b] BET = Brunauer–Emmett–Teller, *SSA* = specific surface area. [c] BJH = Barrett-Joyner-Halenda. [d] DFT = Density Functional Theory, *SPV* = specific pore volume.

nitrogen adsorption at 77 K with a surface area and pore size analyser (3Flex 3500, Micromeritics Instrument Corp., USA). The samples were vacuum degassed at 350°C for 3 – 5 days using a degasser (VacPrep 061, Micromeritics Instrument Corp., USA) and then in-situ degassed at 350°C for 20 h by a turbo molecular drag pump prior to the analyses. Based on the isothermal plots (Fig. 6), the *SSA* and *SPV* of the PACs were obtained by various models and shown in Table 2. The BET method was used for the overall *SSA* analysis. DFT was used to calculate the overall *SPV* (pore sizes of those bigger than 0.393 nm). The *SSA* and *SPV* of meso-macropores were obtained from the BJH theory (pore sizes of 2 – 300 nm). The DFT model was used for determining the *SSA* and *SPV* of micropore (pore sizes of 0.393 – 2.002 nm).

Conclusions

Self-activation is an effective activation process for activated carbon from biomass. The activated carbons were successfully produced without any additional activating gases or chemicals. A model of the activation process was developed to understand and explain the self-activation process. In the study of self-activation of kenaf core, the suggested pyrolysis temperature for the self-activation process is between 970 – 1,090°C, and the most effective pyrolysis temperature is expected to be around 1,090°C. The relationships between yields and specific surface areas (SSA_{BET}), specific pore volumes (SPV_{DFT}, $SPV_{BJH\ meso\text{-}macropore}$, and $SPV_{DFT\ micropore}$) were investigated, i.e. a lineal fitting between ln(SSA_{BET}) and yields, power fittings between SPV_{DFT}, $SPV_{BJH\ meso\text{-}macropore}$ and yields, and a second-order fitting between $SPV_{DFT\ micropore}$ and yields. The changes of specific surface areas (SSA_{BET}, $SSA_{BJH\ meso\text{-}macropore}$, and $SSA_{DFT\ micropore}$) and specific pore volumes (SPV_{DFT}, $SPV_{BJH\ meso\text{-}macropore}$, and $SPV_{DFT\ micropore}$) as a function of pyrolysis temperatures and dwelling times agree with our model prediction. In the analysis of these relationships, the PACs (700-850°C, 10 h; 1,000°C, 100 h) and ash were not included. In addition, the study of the effectiveness of kenaf core for producing highest total surface area showed that the yield of 9.0% received a maximum surface area per using gram kenaf core, and the yields between 5.5% and 13.8% were recommended for more than 90% of effectiveness.

Acknowledgements

This work was supported in part by National Science Foundation (NSF) CMMI 1247008, and University of North Texas Research initiation Fund. We thank Dr. Liping Cai (Mechanical & Energy Engineering, University of North Texas) for the assistance during the project period, Dr. Nandika A. D'Souza (Mechanical & Energy Engineering, University of North Texas) for sharing the lab, Dr. Richard F. Reidy (Materials Science and Engineering, University of North Texas) for help, Dr. Shifeng Zhang (College of Material Science and Technology, Beijing Forestry University) for the ultimate analysis, Dr. Guido F. Verbeck and Mr. Phillip M. Mach (Department of Chemistry, University of North Texas) at the Laboratory of Imaging Mass Spectrometry (LIMS) for the FT-IR and MS tests, and Angela Nelson (College of Engineering, University of North Texas) for proof reading.

Notes and references

1 D. Mohan and C. U. Pittman Jr, *J. Hazard. Mater.,* 2006, **137**, 762–811.
2 Z. H. Hu, M. P. Srinivasan and Y. M. Ni, *Adv. Mater.,* 2000, **12**, 62–65.
3 J. Blanco, A. L. Petre, M. Yates, M. P. Martin, S. Suarez and J. A. Martin, *Adv. Mater.,* 2006, **18**, 1162–1165.
4 M. Pang, C. Liu, W. Xia, M. Muhler and C. Liang, *Green Chem.,* 2012, **14**, 1272–1276.
5 Z. Li, S. Kelkar, L. Raycraft, M. Garedew, J. E. Jackson, D. J. Miller and C. M. Saffron, *Green Chem.,* 2014, **16**, 844–852.
6 K. Fabičovicová, O. Malter, M. Lucas and P. Claus, *Green Chem.,* 2014, **16**, 3580–3588.
7 H. Wang, Q. Gao and J. Hu, *J. Am. Chem. Soc.,* 2009, **131**, 7016–7022.
8 J. Wang, I. Senkovska, S. Kaskel and Q. Liu, *Carbon,* 2014, **75**, 372–380.
9 R. Elazari, G. Salitra, A. Garsuch, A. Panchenko and D. Aurbach, *Adv. Mater.,* 2011, **23**, 5641–5644.
10 S. S. Manickam, U. Karra, L. Huang, Nhu-Ngoc Bui, B. Li and J. R. McCutcheon, *Carbon,* 2013, **53**, 19–28.
11 H. Zhang, Y. Yan and L. Yang, *Adsorption,* 2010, **16**, 161–166.
12 A. C. Lua and T. Yang, *J. Colloid Interf. Sci.,* 2004, **274**, 594–601.
13 B. Xu, Y. Chen, G. Wei, G. Cao, H. Zhang and Y. Yang, *Mater. Chem. Phys.,* 2010, **124**, 504–509.
14 L. Liu, Q. Deng, Y. Liu, T. Ren and Z. Yuan, *Catal. Commun.,* 2011, **16**, 81–85.
15 Ö Gerçel and H. F. Gerçel, *Chem. Eng. J.,* 2007, **132**, 289–297.
16 P. Alvarez, C. Blanco and M. Granda, *J. Hazard. Mater.,* 2007, **144**, 400–405.
17 C. Moreno-Castilla, M. Ferro-Garcia, J. Joly, I. Bautista-Toledo, F. Carrasco-Marin and J. Rivera-Utrilla, *Langmuir,* 1995, **11**, 4386–4392.
18 M. Benadjemia, L. Millière, L. Reinert, N. Benderdouche and L. Duclaux, *Fuel Process. Technol.,* 2011, **92**, 1203–1212.
19 I. I. Gurten, M. Ozmak, E. Yagmur and Z. Aktas, *Biomass Bioenerg.,* 2012, **37**, 73–81.
20 S. Aber, A. Khataee and M. Sheydaei, *Bioresource Technol.,* 2009, **100**, 6586–6591.
21 K. Gadkaree and M. Jaroniec, *Carbon,* 2000, **38**, 983–993.
22 S. Q. Shi and C. Xia, *US Pat.,* 14/211,357, 2014.
23 C. Bommier, R. Xu, W. Wang, X. Wang, D. Wen, J. Lu, and X. Ji, *Nano Energy*, 2015, **13**, 709–717.
24 M. A. Yahya, Z. Al-Qodah, and C. W. Z. Ngah, *Renew. Sust. Energ. Rev.,* 2015, **46**, 218–235.
25 H. Yang, R. Yan, H. Chen, D. H. Lee and C. Zheng, *Fuel,* 2007, **86**, 1781–1788.
26 T. Y. Zhang, W. P. Walawender, L. T. Fan, M. Fan, D. Daugaard and R. C. Brown, *Chem. Eng. J.,* 2004, **105**, 53–59.
27 M. D. Nayeri, P. M. Tahir, J. Harun, L. C. Abdullah, E. S. Bakar, M. Jawaid and F. Namvar, *Bioresources,* 2013, **8**, 1801–1812.
28 UNIQUE project, http://www.uniqueproject.eu/public/deliverables/D5.3.pdf, Accessed 2015-9-9.
29 C. W. Bale, P. Chartrand, S. A. Degterov, G. Eriksson, K. Hack, R. Ben Mahfoud, J. Melançon, A. D. Pelton and S. Petersen, *Calphad,* 2002, **26**, 189–228.
30 O. Senneca, *Fuel Process. Technol.,* 2007, **88**, 87–97.
31 P. Ollero, A. Serrera, R. Arjona, S. Alcantarilla, *Fuel,* 2002, **81**, 1989–2000.
32 P. Ollero, A. Serrera, R. Arjona, S. Alcantarilla, *Biomass Bioenerg.,* 2003, **24**, 151–161.
33 W. Klose, M. Wolki, *Fuel,* 2005, **84**, 885–892.
34 A. M. Khah, R. Ansari, *Int. J. Chem. Technol. Res.,* 2009, **1**, 859–864.
35 K. Matsumoto, K. Takeno, T. Ichinose, T. Ogi, M. Nakanishi, *Fuel,* 2009, **88**, 519–527.

Self-activation for activated carbon from biomass: Theory and parameters

*Changlei Xia and Sheldon Q. Shi**

Department of Mechanical and Energy Engineering, University of North Texas, Denton, TX 76203, USA. E-mail: Sheldon.Shi@unt.edu

Graphical Abstract

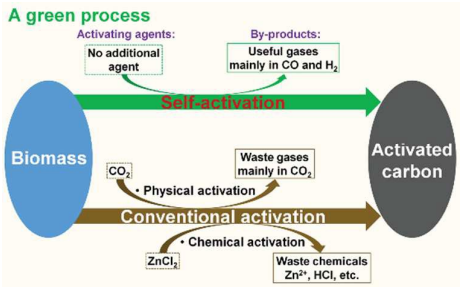

Self-activation is a process taking advantage of gases emitted from the pyrolysis of biomass to activate the converted carbon.